Applied Geochemistry 26 (2011) 884–897

Contents lists available at ScienceDirect

Applied Geochemistry

journal homepage: www.elsevier.com/locate/apgeochem

Geochemical evolution of groundwater in carbonate aquifers in Taiyuan, northern China

Rui Ma [a,b,*], Yanxin Wang [a], Ziyong Sun [a], Chunmiao Zheng [b], Teng Ma [a], Henning Prommer [c,d]

[a] School of Environmental Studies & MOE Key Laboratory of Biogeology and Environmental Geology, China University of Geosciences, 430074 Wuhan, PR China
[b] Department of Geological Sciences, The University of Alabama, Tuscaloosa, AL 35487, United States
[c] CSIRO Land and Water, Floreat, Australia
[d] School of Earth and Environment, University of Western Australia, Crawley, Western Australia, Australia

ARTICLE INFO

Article history:
Received 3 September 2010
Accepted 22 February 2011
Available online 21 March 2011
Editorial handling by D. Gooddy

ABSTRACT

Thirty-nine samples of both cold and thermal karst groundwater from Taiyuan, northern China were collected and analyzed with the aim of developing a better understanding of the geochemical processes that control the groundwater quality evolution in the region's carbonate aquifers. The region's karst groundwater system was divided into three geologically distinct sub-systems, namely, the Xishan Mountain karst groundwater subsystem (XMK), the Dongshan Mountain karst groundwater subsystem (DMK) and the Beishan Mountain karst groundwater subsystem (BMK). Hydrochemical properties of the karst groundwaters evolve from the recharge zones towards the cold water discharge zones and further towards the thermal water discharge zones. In the XMK and the DMK, the hydrochemical type of the groundwater evolves from HCO_3–Ca·Mg in the recharge – flow-through zone, to HCO_3·SO_4–Ca·Mg/SO_4·HCO_3–Ca·Mg in the cold water discharge zone, and further to SO_4–Ca·Mg in the thermal water discharge zone. By contrast, the water type changes from HCO_3–Ca·Mg to HCO_3·SO_4–Ca·Mg in the BMK, with almost invariable TDS and temperatures all along from the recharge to the discharge zone. The concentrations of Sr, Si, Fe, F^- and of some trace elements (Al, B, Li, Mn, Mo, Co, Ni) increase as groundwater temperature increases. Different hydrogeochemical processes occur in the three karst groundwater sub-systems. In the XMK and the DMK, the geochemical evolution of the groundwater is jointly controlled by carbonate dissolution/precipitation, gypsum dissolution and dedolomitization, while only calcite and dolomite dissolution/precipitation occurs in the BMK without dedolomitization. The hydrogeochemical data of the karst groundwaters were used to construct individual geochemical reaction models for each of the three different karst groundwater sub-systems. The modeling results confirm that dedolomization is the major process controlling hydrochemical changes in the XMK and the DMK. In the thermal groundwaters, the dissolution rates of fluorite, siderite and strontianite were found to exceed those of the cold karst groundwater systems, which can explain the higher concentrations of F^-, Fe and Sr^{2+} that are found in these waters.

1. Introduction

As one of the most important water supply sources worldwide, groundwaters with low temperature from carbonate aquifers have significant value and karst aquifers have been the subject of geochemical investigations since the 1970s. As a result, geochemical processes in carbonate aquifer systems and their hydrogeological implications are now well documented for many different sites worldwide (e.g., Hanshaw and Back, 1979; Plummer et al., 1990; Hess and White, 1993; Wicks and Herman, 1996; Stetzenbach et al., 1999; Capaccioni et al., 2001; Grasby and Betcher, 2002; Jacobson and Wasserburg, 2005; McIntosh and Walter, 2006; Wang et al., 2006; Dobrzyński, 2007; Moral et al., 2008; Kohfahl et al., 2008). The investigation and understanding of geochemical processes that control groundwater evolution in such aquifers provide essential information for understanding the sustainability of groundwater extractions and to support the regulatory frameworks that control groundwater exploitation. This is particularly important in such area as northern China, where groundwater supply accounts for 78% of the total water supply.

Located in the arid-semi-arid region of northern China, Taiyuan City, with a population of 3.5 million, is suffering a serious shortage of water resources. For decades groundwater from carbonate aquifers has been one of the most important sources of water supply and the sustainable exploitation of the karst groundwater has always been a major concern for the local government (Han et al., 1993; He and Xu, 1993; He et al., 1997).

* Corresponding author at: School of Environmental Studies, China University of Geosciences, 430074 Wuhan, PR China.
E-mail address: ruima79@gmail.com (R. Ma).

0883-2927/$ - see front matter © 2011 Elsevier Ltd. All rights reserved.
doi:10.1016/j.apgeochem.2011.02.008

Being a major water supply source for Taiyuan, the Ordovician carbonate aquifer has been extensively studied at both local and regional scales since the 1960s. For example, Zhao and Cai (1990) investigated the lithology, geological structure and karst development features of the carbonate aquifer and analyzed the prevailing major groundwater flow patterns. He et al. (1997) further documented the recharge, flow and discharge information of groundwater from carbonate aquifers and assessed the quality of the groundwaters. The groundwater flow was also studied at the western and eastern parts of the Taiyuan carbonate aquifer, respectively (Ha et al., 1989; Wang and Wang, 1990; Zhang, 1990, 1993).

Some research has been dedicated to geochemical and isotopic investigations whereby the geochemical data were used to elucidate the groundwater recharge and flow patterns (Zhang, 1993; He et al., 1997). Xu et al. (1987) studied the hydrogeochemical characteristics of the groundwater at the western part of the carbonate aquifer and concluded that the geochemical evolution of the karst groundwaters was mainly controlled by carbonate and gypsum dissolution. The study of Han et al. (1993) indicated that sulfate mineral dissolution may promote calcite precipitation in the western part of the Ordovician carbonate aquifer in Taiyuan. Overall, all the cited studies focused on cold karst groundwaters with temperatures remaining below 25 °C. In 1995, thermal groundwaters with temperatures above 30 °C were discovered in the deeper Ordovician carbonate aquifers of Taiyuan. Since then, 17 deep boreholes have been drilled to abstract thermal karst groundwater. However, since the cold karst groundwaters and the thermal karst groundwaters are extracted from the same Ordovician carbonate aquifer this raised intense arguments regarding the potential for over-exploitation of the aquifer by using the thermal groundwater resources. For a sustainable development of the groundwater resources in carbonate aquifers it is now vitally important to understand the origin of the thermal karst groundwaters, This can only be achieved if it is understood how water–rock interactions affect the compositional evolution of the waters between recharge and discharge zones. Because of the diversity of the hydrogeological and hydrochemical conditions, Zhao and Cai (1990) and He et al. (1997) divided karst water systems in Taiyuan into three regional subsets based on geological structures, hydrogeological and geochemical data. Apart from this, no systematic hydrogeochemical studies of both cold groundwater and thermal groundwater has previously been conducted and no consistent conceptual model of the geochemical processes that control groundwater evolution in the carbonate aquifers in Taiyuan has been developed.

The objective of this study is to fill this knowledge gap by an integrated analysis of all available hydrochemical data and, based on this, to develop quantitative mass transfer models that represent all major flow and reaction pathways.

2. Regional hydrogeology

Taiyuan city, the capital of the Shanxi Province in northern China, is located in the Taiyuan Quaternary Basin, surrounded by Xishan (west) Mountain, Dongshan (east) Mountain and Beishan (north) Mountain (Fig. 1). The study area has a semi-arid climate with a mean annual temperature of about 8 °C, a mean annual rainfall of 449.7 mm in the past 40a, and an annual evaporation of 1045 mm. The total abstraction of karst groundwater is 1.4×10^8 m^3/a. Groundwater levels have been declining continuously over the past 40a as a result of excessive pumping.

The main outcropping strata in the mountain areas include Archean metamorphic rocks, Cambrian carbonate rocks, Ordovician carbonate rocks, Carboniferous coal-bearing clastic rocks, and Permian and Triassic clastic rocks. The strata extend underneath the Taiyuan Basin and are overlain by Tertiary and Quaternary sediments.

The middle series of Ordovician carbonate rocks is the main aquifer for water supply at Taiyuan and consists of calcite, dolomite, and marl with thick interlayers of gypsum and minor amounts of minerals such as fluorite and halite (Ha et al., 1989; Zhao and Cai, 1990; Zhang, 1993; Wu, 1997; He et al., 1997). The karstification of the Cambrian dolomitic limestone is much less intense than that of the Ordovician carbonate rocks.

Based on the structural geology, combined with hydrogeological as well as hydrogeochemical information the studies of Zhao and Cai (1990) and He et al. (1997) divided the whole karst groundwater system into three sub-systems, namely the Xishan Mountain karst groundwater subsystem (XMK), the Dongshan Mountain karst groundwater subsystem (DMK) and the Beishan Mountain karst groundwater subsystem (BMK). The boundaries delineating these sub-systems are shown in Fig. 1. The XMK study area, in the northwestern part of the mountain, is mainly a karst terrain bounded by metamorphic rocks on the north and west, the Liulin valley on the NE and the peripheral fault zone on the east and SE (Fig. 1). In the XMK, the carbonate rocks range from Cambrian to Middle Ordovician in age and are underlain by impermeable Precambrian metamorphic rocks which are exposed along the northern fringe. The BXK is bounded by metamorphic rocks on the north and by the Sangei Horst on the south. It shares the west and east boundaries with the XMK and the DMK. The DXK is bounded by an anticline on the SE and metamorphic rocks on the NE.

The karst groundwater system receives recharge mostly from atmospheric precipitation in carbonate outcrop areas NW, north and NE of Taiyuan, and partly from leakage of surface runoff (Zhao and Cai, 1990). The Fenhe River runs for about 30 km across carbonate rocks where it strongly interacts with the karst groundwater system. For the SW, central north and SE zones of Taiyuan where the carbonate rocks are overlain by thick layers of massive sandstone and shale of the Carboniferous, Permian and Triassic and unconsolidated sediments of Tertiary and Quaternary, vertical recharge of atmospheric precipitation is minimal. In this zone, the carbonate aquifers are confined and constitute the flow-through zone of the regional karst groundwater system. Under natural conditions, the dominant mode of regional drainage of the carbonate aquifers is via karst springs, namely, the Lancun Spring and the Jinci Spring. However, due to the decade-long over-exploitation of groundwater at Taiyuan, the Lancun Spring ceased outflow in 1988 and the Jinci Spring in 1994. Consequently, pumping became the major means of discharge for the karst groundwaters. The general direction of regional groundwater flow in carbonate aquifers is from the NW, through the SW, to the margin of the Xishan Mountain in the XMK; from the NW, north and NE, through the central north, to the south in the BMK; and from NE to the margin of the Dongshan Mountain in the DMK (Fig. 1). Complex tectonic structures and folded and faulted structures have been recognized at Taiyuan (Fig. 1). The faults at the margin of the Xishan Mountain, the Dongshan Mountain and the Beishan Mountain function as the main passage for karst groundwater discharge, where karst groundwater from depth flows vertically upwards or permeates into the Quaternary aquifers of the Taiyuan basin.

3. Data collection, sampling and analysis

A total of 39 karst groundwater samples from public supply wells and industry wells were collected in the study area between April 20, 2006 and July 23, 2006. Among the samples, 38 were from the Middle Series of the Ordovician carbonate aquifer and one (sample No. RN32) from the upper Cambrian carbonate aquifer. The sampling locations and hydrochemistry of the samples are

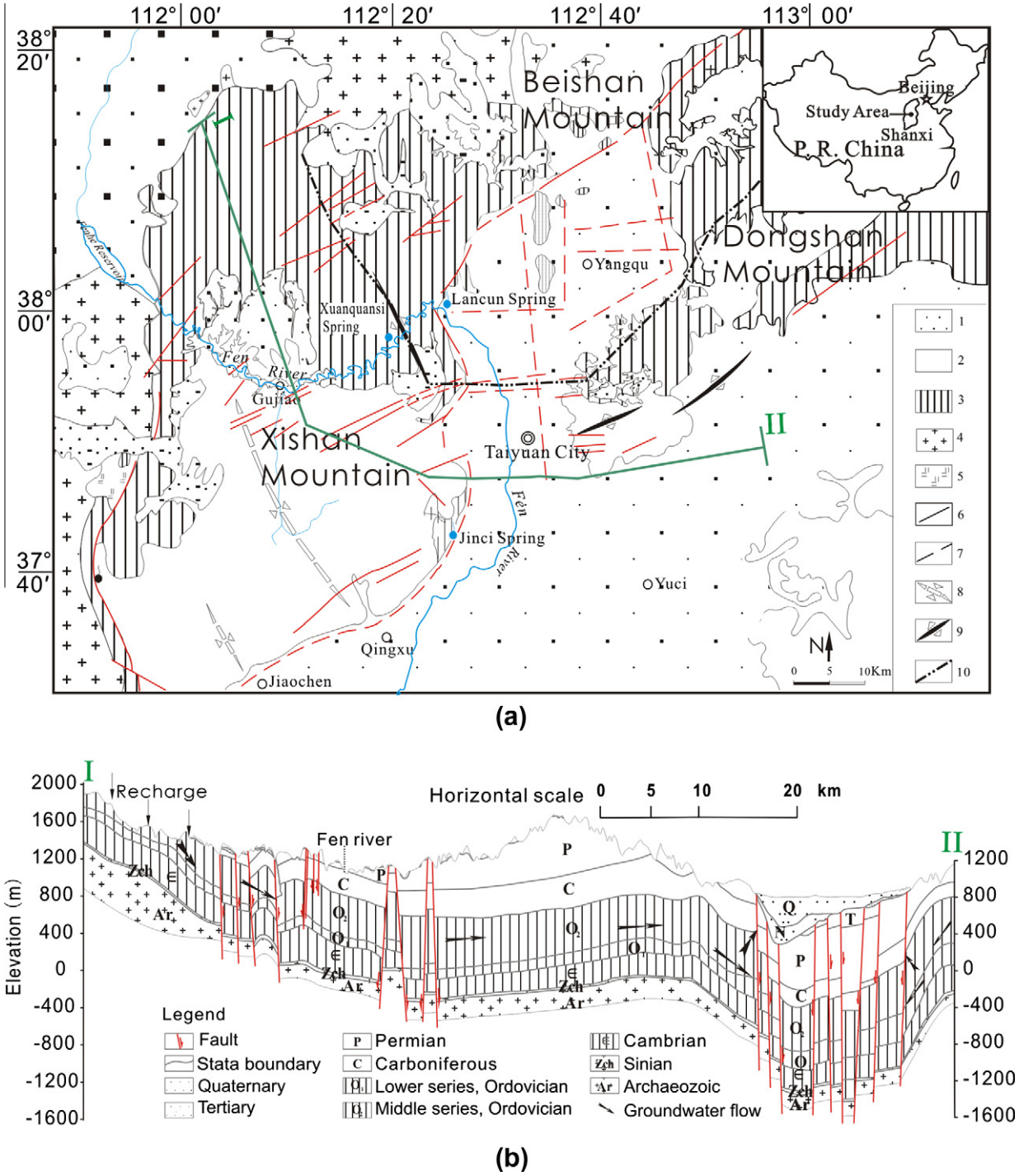

Fig. 1. (a) Simplified geological map of Taiyuan, China: (1) Tertiary and Quaternary unconsolidated sediments; (2) Carboniferous, Permian and Triassic clastic rocks; (3) upper Cambrian and Ordovician carbonate rocks; (4) Archean and Sinian metamorphic rocks; (5) igneous rocks; (6) fault; (7) buried fault; (8) syncline; (9) anticline; (10) boundary between Dongshan Mountain, Beishan Mountain and Xishan Mountain karst water subsystems (respectively abbreviated as DMK, BMK and XMK in the text). (b) The hydrogeological section along the I and II line.

shown in Fig. 2 and Table 1, respectively. All available boreholes of the system were sampled. Before sampling, clean polypropylene sample bottles were rinsed in deionized water. Waters were sampled after pumping for at least 30 min. Temperature, pH and electrical conductivity (EC) were measured in the field using portable Hanna EC and pH meters, which had been calibrated before use. Alkalinity was measured on the sampling day using the Gran titration method. Water samples were filtered through 0.45 μm membranes in the field. Samples were collected in three new 500 mL polyethylene bottles. Samples for cation and trace element analysis were acidified (with ultrapure HNO_3 to pH = 2). Anions (SO_4^{2-}, Cl^-, NO_3^-, F^-) were determined using ion chromatography (model DX-120, Dionex), while cations (Ca^{2+}, Mg^{2+}, K^+, Na^+) and some minor elements (Si, Sr^{2+}, Fe) were determined by ICP–AES (IRIS INTRE II XSP). Trace elements were determined by ICP–MS (Agilent 7500a plasma mass spectrometer) within 2 weeks of sampling. The uncertainties of measurements for major and trace elements are all within 5%. The results are given in Table 1.

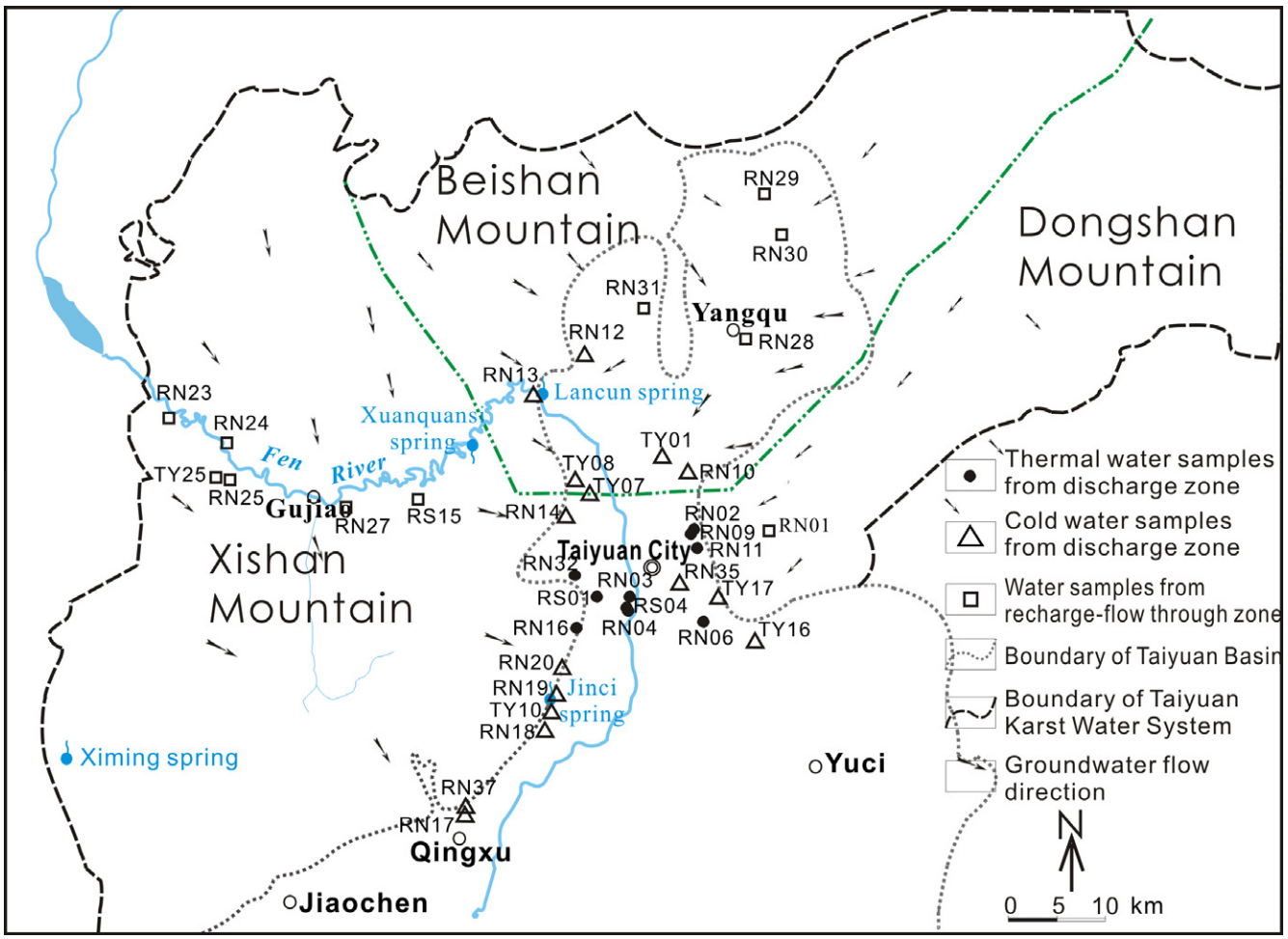

Fig. 2. Karst water flow directions and sampling locations.

Mineral saturation indices and CO_2 partial pressures for the carbonate groundwaters of Taiyuan were calculated with PHREEQC 2.15 (Parkhurst and Appelo, 1999). PHREEQC2-15 was also used to model the chemical evolution associated with water/rock interactions in the Taiyuan carbonate aquifer system, and to describe the observed chemical composition of aqueous and solid phases.

4. Results

4.1. Hydrochemistry of karst groundwater

4.1.1. Major ions

As a first step, the karst groundwater samples were plotted onto Piper's diagrams (Figs. 3a–c). This allowed further classification of the water samples from each subsystem into three major groups according to their location on the Piper's diagrams and their hydrogeological environments.

4.1.1.1. Xishan Mountain karst groundwater subsystem (XMK, Fig. 3a). Group A includes samples from the recharge and flow-through zones in the NW or west part of the XMK. The water types are HCO_3–Ca or HCO_3–Ca·Mg in the recharge zone and HCO_3·SO_4–Ca·Mg in the flow-through zone. The TDS of these samples is less than 500 mg/L, the temperature ranges from 13.6 °C to 17.3 °C, the pH between 6.4 and 7.58 and the conductivity between 432 μS/cm and 721 μS/cm. The water sample RN27 is from the local discharge zone of the XMK and its chemical composition is similar to that of the cold waters from the flow-through zone.

Group B includes water samples from shallow wells (100–300 m deep) that are distributed mainly along the fault zone at the margin of the Xishan Mountain. The water samples indicate predominantly HCO_3·SO_4–Ca·Mg and SO_4·HCO_3–Ca·Mg type waters, with temperatures ranging from 12.2 to 25 °C, pH from 6.89 to 7.79, conductivity from 982 to 1460 μS/cm, and with TDS between 638 and 1135 mg/L. The chemical composition of water sample RN14 from the local discharge zone (temperature = 12.2 °C; EC = 982 μS/cm; pH = 6.89; TDS = 638 mg/L) is similar to those of the waters from the flow-through zone.

Group C includes thermal groundwaters from depths of 600–2000 m that were collected along the NE fault zone in the eastern margin of the Xishan Mountain and from buried Ordovician aquifers. They are characterized by elevated temperatures ranging from 30 up to 62.5 °C. The major hydrochemical type is SO_4–Ca·Mg, with TDS of 1661 ~2279 mg/L, pH of 6.71–7.33 and conductivities commonly >2200 μS/cm. These waters contain the highest SO_4^{2-} concentrations (>1000 mg/L) of all the samples collected from Taiyuan. Compared to the samples from the Ordovician carbonate aquifer, sample RN32 from the Cambrian carbonate aquifer has a distinctly different character: it is a HCO_3·SO_4 water with the lowest temperature (30 °C), an EC of 1082 μS/cm and a TDS of 596 mg/L.

Table 1
Chemical properties and composition of karst water samples from Taiyuan.

Karst water subsystem		Sample no.	Borehole depth (m)	Physicochemistry			Major elements (mg/L)									Minor elements (mg/L)			
				T (°C)	pH	EC (μs/cm)	CO_3^{2-}	HCO_3^-	F^-	Cl^-	NO_3^-	SO_4^{2-}	Ca^{2+}	Mg^{2+}	Na^+	K^+	Fe	Si	Sr
DMK	Recharge and flow-through zone	RN01	570	16.0	7.74	482	n.d.	276.53	0.36	5.34	13.02	23.52	54.78	24.10	10.97	0.28	0.15	4.29	0.61
DMK	Cold water discharge zone	RN35	1100	23.0	6.80	700	n.d.	286.79	1.38	9.51	5.46	206.90	90.91	44.60	14.89	1.45	0.21	4.17	1.54
DMK		TY16	800	24.7	7.27	892	n.d.	285.18	0.44	24.00	5.83	268.10	123.50	47.32	24.33	3.04	–	5.49	4.92
DMK		TY17	960	18.7	7.30	923	n.d.	305.00	0.41	26.23	9.43	290.90	139.40	41.30	34.03	0.73	–	4.73	2.39
DMK	Thermal water discharge zone	RN02	1150	30.0	7.60	985	n.d.	325.15	1.91	14.91	n.d.	221.37	108.04	44.93	26.83	2.04	2.70	5.09	3.24
DMK		RN06	1168	30.0	7.09	1130	n.d.	284.13	1.75	13.73	1.71	382.95	151.67	53.81	26.78	1.26	0.50	5.44	3.25
DMK		RN09	1351	33.4	7.05	1630	n.d.	243.41	1.82	35.00	n.d.	739.25	227.31	75.07	44.22	4.02	2.81	6.69	6.26
DMK		RN11	1250	34.0	7.27	1150	n.d.	270.45	1.85	12.63	n.d.	364.00	157.42	55.53	19.48	1.97	1.58	5.97	2.85
BMK	Recharge and flow-through zone	RN28	790	17.3	7.17	420	n.d.	292.24	n.d.	5.02	10.59	12.40	52.20	23.66	10.95	0.50	0.06	3.70	0.43
BMK		RN29	500	18.4	6.90	396	n.d.	268.62	n.d.	8.25	8.47	25.70	49.66	25.29	14.15	0.67	0.07	4.41	0.45
BMK		RN30	601.37	14.8	6.57	414	n.d.	389.66	n.d.	7.07	34.24	16.00	75.11	35.36	15.18	0.67	0.06	4.87	0.74
BMK		RN31	460	16.0	6.89	386	n.d.	284.68	n.d.	6.44	12.02	9.10	52.27	22.11	14.39	0.61	0.01	3.97	0.27
BMK	Cold water discharge zone at the margin of the mountain	RN10	550	16.9	7.21	455	n.d.	274.40	n.d.	6.08	10.27	14.74	57.70	23.31	8.94	n.d.	n.d.	4.03	0.45
BMK		RN12	300	14.7	7.28	422	n.d.	273.80	n.d.	6.35	8.09	7.76	52.25	22.74	9.87	n.d.	0.08	3.83	0.29
BMK		RN13	300	15.2	7.19	480	n.d.	273.50	0.4	8.13	9.69	32.44	56.29	24.35	12.16	n.d.	n.d.	3.94	0.54
BMK	Cold water discharge zone in buried karst zone	TY01	830	14.0	6.59	472	n.d.	286.70	0.08	11.87	16.91	135.10	106.90	23.10	10.16	0.56	–	5.09	0.60
BMK		TY07	600	14.0	7.60	551	n.d.	237.90	0.35	26.55	12.47	81.28	82.95	24.00	16.92	0.56	–	4.51	0.81
BMK		TY08	600	15.0	7.74	533	n.d.	237.90	0.26	25.07	12.07	66.21	80.45	22.41	17.31	0.91	–	4.48	0.69
XMK	Recharge and flow-through zone	RN23	330	16.8	7.00	460	n.d.	214.59	n.d.	13.75	10.85	57.74	51.75	17.28	19.49	2.08	n.d.	3.35	0.38
XMK		RN24	500	13.6	6.40	432	n.d.	241.61	n.d.	12.75	11.09	110.50	73.92	23.84	17.21	1.12	n.d.	3.91	0.49
XMK		RN25	468	16.9	6.69	451	n.d.	225.40	n.d.	7.97	6.45	101.72	63.08	25.32	13.09	0.87	n.d.	4.08	0.78
XMK		RN27	179	15.2	6.60	715	n.d.	266.31	n.d.	46.70	16.69	221.72	116.50	33.98	30.67	1.51	0.27	4.14	0.77
XMK		TY25	500	16.5	7.58	536	n.d.	237.70	0.40	8.83	9.73	108.20	89.89	26.39	12.22	0.88	–	5.19	0.84
XMK		RS15	172	17.3	7.33	721	n.d.	268.49	n.d.	47.46	13.00	114.41	78.28	22.80	29.09	1.17	0.02	3.55	0.93
XMK	Cold water discharge zone	RN14	580	12.2	6.89	982	n.d.	372.25	n.d.	27.57	3.60	217.58	123.60	43.89	35.12	0.60	2.73	3.70	1.00
XMK		RN17	100	24.0	7.00	1460	n.d.	241.58	0.56	12.42	n.d.	672.75	235.14	69.74	22.00	0.48	0.39	3.97	2.82
XMK		RN18	100	17.9	7.48	1077	n.d.	256.78	n.d.	15.42	5.15	341.48	137.63	43.03	38.43	0.08	0.20	4.11	2.04
XMK		RN19	154	19.4	7.00	1080	n.d.	239.31	n.d.	16.23	13.89	378.65	150.43	48.27	19.11	0.81	n.d.	4.14	3.00
XMK		RN20	100	20.8	7.09	1002	n.d.	243.10	n.d.	15.06	5.11	296.78	137.84	43.93	18.26	1.13	n.d.	4.23	3.48
XMK		RN37	100	27.0	7.20	1300	n.d.	231.88	1.42	12.84	10.85	673.80	228.90	69.96	20.00	1.61	0.23	4.00	3.37
XMK		TY10	230	19.5	7.79	1050	n.d.	230.28	0.53	17.46	11.06	461.10	176.00	47.02	24.45	2.51	–	5.11	3.93
XMK	Thermal water discharge zone	RN32	2000	30.0	6.88	1083	n.d.	311.85	n.d.	77.57	n.d.	172.30	112.78	47.20	28.08	2.14	5.20	7.08	11.33
XMK		RN03	1805	60.0	7.33	2260	n.d.	262.25	2.40	8.46	n.d.	1172.70	387.08	97.97	15.16	7.27	21.14	8.23	4.41
XMK		RN04	1803	62.5	6.97	3000	n.d.	227.61	2.39	8.51	n.d.	1077.30	347.58	88.96	15.20	7.37	9.60	10.52	5.82
XMK		RN16	603	39.0	6.81	2400	n.d.	237.33	1.26	12.38	n.d.	1366.10	412.11	105.54	25.34	10.20	4.27	9.46	8.27
XMK		RS01	1339	51.0	6.71	2630	n.d.	195.26	2.16	14.20	1.78	1542.30	444.90	119.30	38.26	18.48	0.14	9.99	9.62
XMK		RS04	1600	48.0	6.94	2200	n.d.	237.98	2.20	8.55	n.d.	1462.30	356.70	107.70	19.22	8.44	0.20	8.34	4.87

Karst water subsystem		No.	Trace elements (μg/L)														
			As	Ag	Al	B	Ba	Cd	Co	Cu	Hg	Li	Mn	Mo	Ni	Sb	Zn
DMK	Recharge and flow-through zone	RN01	0.71	0.61	111.00	42.4	110.0	0.024	0.25	3.01	0.072	6.25	0.92	1.37	0.88	2.56	27.00
DMK	Cold water discharge zone	RN35	0.15	0.07	33.10	63.1	110.0	0.019	0.28	0.67	0.024	27.60	9.89	7.54	1.04	1.37	10.00
DMK		TY16	0.15	0.03	–	–	24.0	0.568	0.44	–	0.033	–	18.20	2.61	2.55	–	–
DMK		TY17	0.28	0.01	–	–	26.6	0.621	0.68	–	0.042	0.09	4.31	10.12	3.40	–	–
DMK	Thermal water discharge zone	RN02	0.31	0.31	76.20	73.6	34.0	0.020	0.21	1.20	0.070	38.20	27.10	2.85	0.95	1.81	25.20
DMK		RN06	0.13	0.20	21.10	70.8	28.4	0.015	1.01	0.88	0.041	31.20	12.70	3.77	0.90	8.54	11.00
DMK		RN09	0.28	0.18	92.10	100.0	35.8	0.018	1.42	2.11	0.047	56.80	19.40	0.45	1.21	10.90	10.40

DMK		RN11	0.27	0.23	84.50	67.9	23.4	0.023	0.26	1.25	0.055	33.50	11.20	1.43	1.05	2.07	13.20
BMK	Recharge and flow-through zone	RN28	0.43	0.09	1.95	41.2	78.4	0.020	0.12	6.81	0.031	7.63	0.60	0.97	0.29	1.42	6.24
BMK		RN29	0.43	0.08	14.10	57.9	166.0	0.011	0.13	0.61	0.032	9.32	2.56	1.67	0.33	1.45	1.73
BMK		RN30	0.36	0.06	5.42	64.0	72.2	0.013	0.28	2.60	0.180	12.30	1.74	1.83	1.45	1.64	58.80
BMK		RN31	0.53	0.06	5.39	36.5	46.6	0.007	0.12	0.38	0.018	6.11	0.28	0.97	0.32	1.70	1.73
BMK	Cold water discharge zone at the margin of the mountain	RN10	0.50	0.18	8.64	35.9	136.0	0.018	0.51	7.69	0.058	6.11	0.27	1.75	0.53	4.92	9.18
BMK		RN12	0.42	0.17	11.30	46.9	56.6	0.014	0.59	23.70	0.045	7.26	1.76	0.90	0.50	5.20	8.11
BMK		RN13	0.45	0.11	7.69	44.8	109.0	0.013	0.39	0.59	0.037	7.81	0.50	1.16	0.40	3.56	6.66
BMK	Cold water discharge zone in buried karst zone	TY01	0.55	–	–	–	120.3	0.337	0.60	3.65	0.024	0.05	5.10	1.28	2.82	–	0.56
BMK		TY07	0.44	0.00	–	–	59.1	0.628	0.43	–	0.062	–	0.40	1.62	2.01	–	–
BMK		TY08	0.45	–	–	–	58.1	0.567	0.37	–	0.035	0.01	2.21	1.51	1.69	–	6.67
XMK	Recharge and flow-through zone	RN23	0.33	0.06	2.81	55.9	52.2	0.010	0.16	0.81	0.046	9.06	6.46	1.81	0.53	1.36	37.00
XMK		RN24	0.33	0.05	1.26	43.7	72.3	0.009	0.16	0.50	0.027	12.20	0.18	1.50	0.35	1.21	1.53
XMK		RN25	0.11	0.08	3.51	28.3	24.2	0.012	0.31	0.45	0.026	10.40	2.28	1.79	0.31	2.13	58.80
XMK		RN27	0.44	0.08	6.70	52.6	64.0	0.015	0.27	0.86	0.034	17.50	1.48	1.60	0.62	1.61	5.37
XMK		TY25	0.24	–	–	–	23.7	0.374	0.27	–	–	–	0.73	1.88	1.32	–	–
XMK		RS15	–	–	–	–	–	–	–	–	–	–	–	–	–	–	–
XMK	Cold water discharge zone	RN14	0.19	0.16	14.80	76.6	24.4	0.016	0.61	1.25	0.037	33.00	54.80	0.43	1.50	3.41	107.00
XMK		RN17	0.24	0.30	26.80	92.8	16.9	0.022	0.52	0.81	0.048	30.20	47.90	3.31	2.35	3.60	20.80
XMK		RN18	2.91	0.20	12.20	87.4	23.2	0.019	0.46	1.00	0.046	18.90	21.40	3.40	0.85	2.74	15.10
XMK		RN19	0.18	0.19	6.45	66.3	23.8	0.017	0.68	0.63	0.039	29.90	0.29	2.64	0.95	4.39	14.80
XMK		RN20	0.20	0.13	6.75	68.0	30.4	0.015	0.31	0.51	0.030	37.30	0.34	4.89	0.81	1.71	7.46
XMK		RN37	0.14	0.08	4.35	97.3	14.8	0.014	0.32	0.56	0.016	30.90	12.10	3.42	1.06	0.96	2.76
XMK		TY10	0.30	0.01	–	–	26.6	0.461	0.66	0.50	0.027	0.01	1.81	2.43	3.46	–	0.69
XMK	Thermal water discharge zone	RN32	1.30	0.16	432.00	51.5	121.0	0.024	0.89	1.51	0.064	19.50	79.50	27.30	1.24	2.74	5.75
XMK		RN03	0.21	0.34	34.80	99.8	29.0	0.018	0.37	1.03	0.086	43.80	175.00	0.92	1.45	1.97	14.30
XMK		RN04	0.32	0.29	46.70	108.0	32.2	0.030	0.72	1.73	0.053	49.70	92.60	1.97	2.53	5.24	17.90
XMK		RN16	0.22	0.23	11.30	136.0	19.1	0.019	0.69	1.06	0.028	74.30	83.30	2.60	2.17	3.71	13.60
XMK		RS01	–	–	–	–	–	–	–	–	–	–	–	–	–	–	–
XMK		RS04	–	–	–	–	–	–	–	–	–	–	–	–	–	–	–

–: Not measured; nd: not detected.

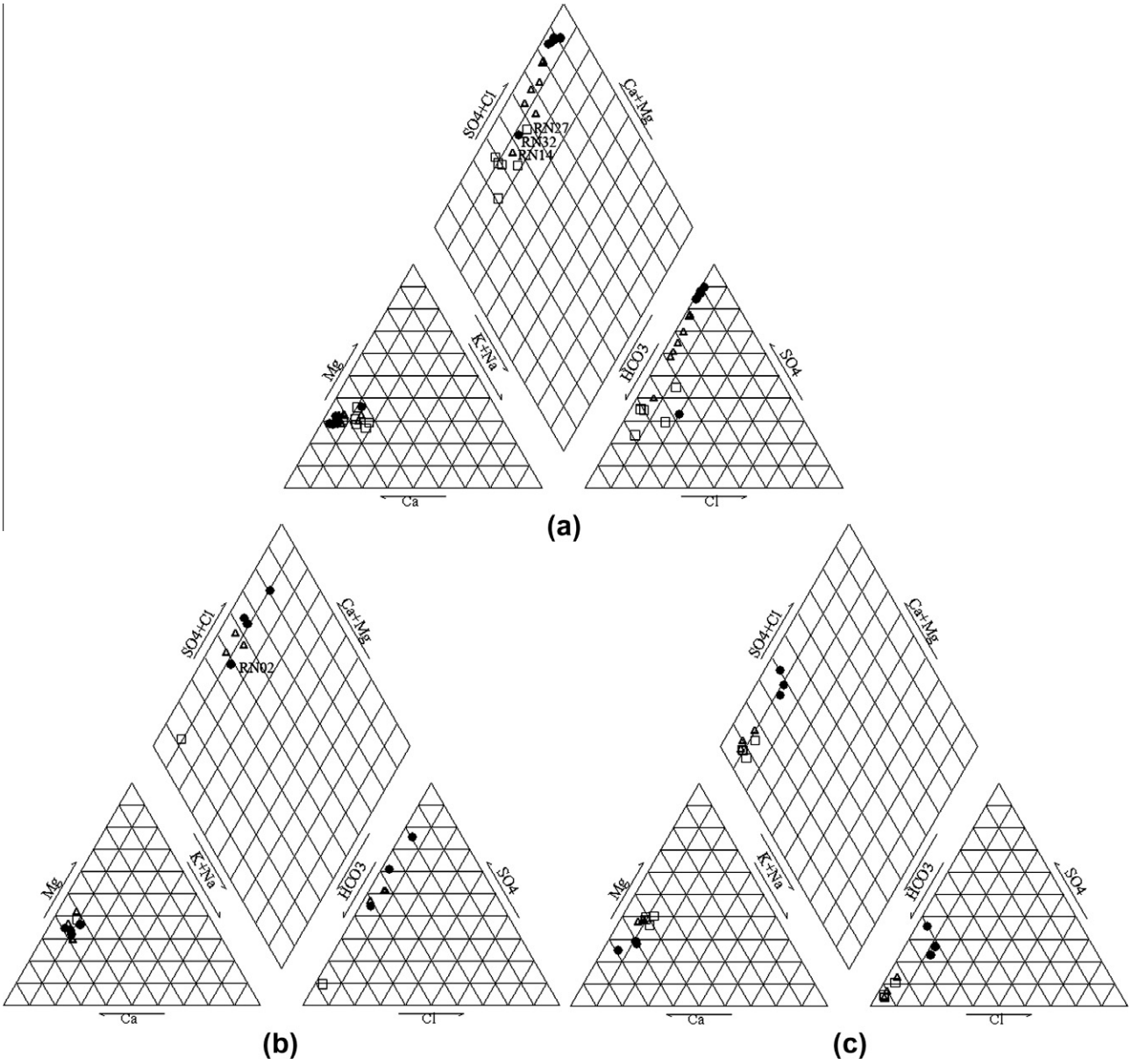

Fig. 3. (a) Piper diagram of karst groundwater samples of XMK. Group A: cold karst groundwater samples from recharge and flow-through zone; Group B: △ cold karst groundwater samples from shallow discharge zone; Group C: ● thermal karst groundwater samples from deep discharge zone. (b) Piper diagram of karst groundwater samples of DMK. Symbols as in Fig. 3a. (c) Piper diagram of karst groundwater samples of BMK. Group A: cold karst groundwater samples from recharge and flow-through zone; Group B: △ cold karst groundwater samples from the discharge zone at the margin of the BMK; Group D: ● cold karst groundwater samples from underlying karst zone in the north part of the basin in the BMK.

4.1.1.2. Dongshan Mountain karst groundwater subsystem (DMK, Fig. 3b). Group A includes only one sample from the NE part of the DMK which cannot be clearly attributed to either the recharge or the flow-through zone. The hydrochemical water type is HCO_3–Ca·Mg, with a TDS of 270.6 mg/L, a temperature of 16 °C, pH of 7.74 and a conductivity of 482 μS/cm.

Group B includes samples from the shallow part near the margin of the DMK, with generally slightly elevated temperatures (mostly between 18.7 and 24.7 °C) compared to those of Group A. The water samples contain higher concentrations of SO_4^{2-} and are HCO_3·SO_4–Ca·Mg or SO_4·HCO_3–Ca·Mg type waters, with a TDS between 518.6 and 695.0 mg/L, pH between 6.8 and 7.3 and conductivities between 700 and 923 μS/cm. The only exception is sample RN02, which has a higher temperature (30 °C) than the rest of the samples of this group.

Group C includes samples from boreholes screened at depths of 1166–1351 m below ground. The boreholes are located along the fault zone at the margin of the DMK. The samples were found to have the highest temperature in the DMK, ranging from 32 to 35 °C. They indicate a SO_4·HCO_3–Ca·Mg or SO_4–Ca·Mg type water with TDS between 748 and 1248 mg/L, pH between 7.05 and 7.6 and conductivities ranging from 1130 to 1630 μS/cm. These waters contain the highest SO_4^{2-} concentration of the DMK samples (>1000 mg/L). The major ion concentrations of the thermal groundwater samples from the DMK are generally less than those from the XMK.

4.1.1.3. Beishan Mountain karst groundwater subsystem (BMK, Fig. 3(c)). Group A includes samples from the flow-through zone of the BMK. The water type is HCO_3–Ca·Mg water with TDS ranging between 259 and 378 mg/L, temperatures between 14.8 and

Table 2
The average saturation indices (SI) of karst groundwater samples in different zones of karst groundwater subsystems in Taiyuan.

Karst water system		Calcite	Aragonite	Dolomite	Gypsum	Anhydrite	Fluorite	CO_2 (g)	Celestite	Strontianite	Siderite	Quartz	Halite	Albite	K-feldspar	K-mica
DMK	Recharge and flow-through zone	0.32	0.17	0.5	−2.31	−2.56	−1.9	−2.37	−2.56	−1.14	−4.5	−0.03	−8.79	−2.64	−1.78	7.44
	Cold water discharge zone	0.23	0.08	0.34	−1.14	−1.38	−1.32	−1.91	−1.09	−0.95	−3.86	−0.08	−7.97	−3.56	−2.21	5.94
	Thermal water discharge zone	0.36	0.22	0.69	−0.93	−1.11	−0.47	−1.80	−0.83	−0.85	−3.32	−0.16	−7.95	−3.29	−2.17	5.84
BMK	Recharge and flow-through zone	−0.47	−0.62	−1.05	−2.51	−2.75	…	−1.46	−2.91	−2.08	−2.88	−0.04	−8.60	−4.04	−2.94	5.08
	Cold water discharge zone	−0.10	−0.25	−0.46	−2.03	−2.28	−2.13	−1.93	−2.44	−1.71	−3.43	−0.01	−8.41	−3.86	…	…
XMK	Recharge and flow-through zone	−0.45	−0.74	−1.16	−1.56	−1.81	−1.64	−1.62	−1.92	−2.01	−3.08	−0.06	−8.04	−4.04	−2.80	5.25
	Cold water discharge zone	0.04	−0.11	−0.15	−0.88	−1.11	−2.40	−1.76	−1.00	−1.31	−2.99	−0.12	−8.02	−3.78	−3.01	4.86
	Thermal water discharge zone	0.34	0.21	0.55	−0.44	−0.51	−0.39	−1.48	−0.34	−0.96	−3.35	−0.16	−8.20	−3.76	−2.22	5.07

Three dots indicate that ion concentration is less than detection limit.

18.4 °C, pH from 6.57 to 7.17 and conductivities ranging from 386 to 420 μS/cm.

Group B includes samples taken from the discharge zone of a shallow part of the Ordovician carbonate aquifer, located along the fault zone at the margin of the BMK. The water type is also HCO_3–Ca·Mg water, with temperatures between 14.7 and 16.9 °C, TDS between 244 and 279.8 mg/L, pH from 7.19 to 7.28, and conductivities ranging from 422 to 480 μS/cm.

Group D includes samples from a buried section of the Ordovician carbonate aquifer in the southern part of the BMK. The water types are either HCO_3·SO_4–Ca·Mg or SO_4·HCO_3–Ca·Mg, with a TDS between 344 mg/L and 448 mg/L, pH from 6.59 to 7.74, conductivities between 472 μS/cm and 533 μS/cm, and temperatures ranging from 14 °C to 15 °C.

The above data indicate that the temperature, conductivity and TDS of groundwater samples from the carbonate aquifer change slightly in different zones of the BMK. It also shows that the major ion concentrations, TDS and conductivities of groundwater samples from the BMK are lower than those from the DMK and the XMK, suggesting that the evolution of groundwater hydrogeochemistry is temperature related.

In general, from the recharge and flow-through zone to the cold water discharge zone, and further to the thermal water discharge zone of the XMK and the DMK, the hydrochemical type of the groundwaters changes from HCO_3 to either HCO_3·SO_4 or SO_4·HCO_3, and further to SO_4 water. At the same time the TDS values increase from initially less than 500 mg/L to about 1000 mg/L, and further to more than 2000 mg/L. The concentrations of SO_4^{2-}, Ca^{2+} and Mg^{2+} also increase along the groundwater flow path, while that of HCO_3^- remains relatively invariable. The spatial distribution of the major ion concentrations confirmed the results of Ma et al. (submitted for publication) which indicates, from the combined analysis of hydrogeological and isotopic data, that cold groundwater in the discharge must originate from the recharge zones of the local groundwater flow systems while the thermal groundwaters are associated with the regional groundwater flow systems.

4.1.2. Minor and trace elements

The measured data indicate that the concentrations of both minor and trace elements in the thermal groundwater clearly exceed those in the cold groundwater. Table 1 shows a comparison for the concentrations of Si, Sr, Fe, F, Ag, Al, B, Co, Cu, Li, Mn and Ni. The data also illustrate that the concentrations of these elements increase successively from the recharge to the flow-through zone and the cold water discharge zone. They are highest in the samples from the thermal groundwater discharge zone in the XMK and the DMK. The contents of other elements such as As, Ba, Cd, Hg, Mo, Sb and Zn are commonly lower and vary slightly from zone to zone. The overall difference in the minor element concentrations between thermal and cold groundwaters indicates that thermal waters have a greater reactivity leading to increased weathering of the minor elements from the host rock during deep circulation. In addition to the increased reactivity of the thermal waters the concentration contrast is presumably amplified by the shorter residence times of the colder groundwaters and their dilution by phreatic or river waters (Wang and Shpeyzer, 1997).

4.2. Saturation indices of minerals

As shown in Table 2, the CO_2 partial pressure decreased successively from the recharge zone towards the cold karst groundwater discharge zone. In the XMK pressures increased again in the thermal karst groundwater discharge zone. In contrast, a steady increase between the recharge and discharge zones was found for the DMK and a constantly decreasing trend was found for the BMK. Table 2 also shows that some waters are oversaturated with

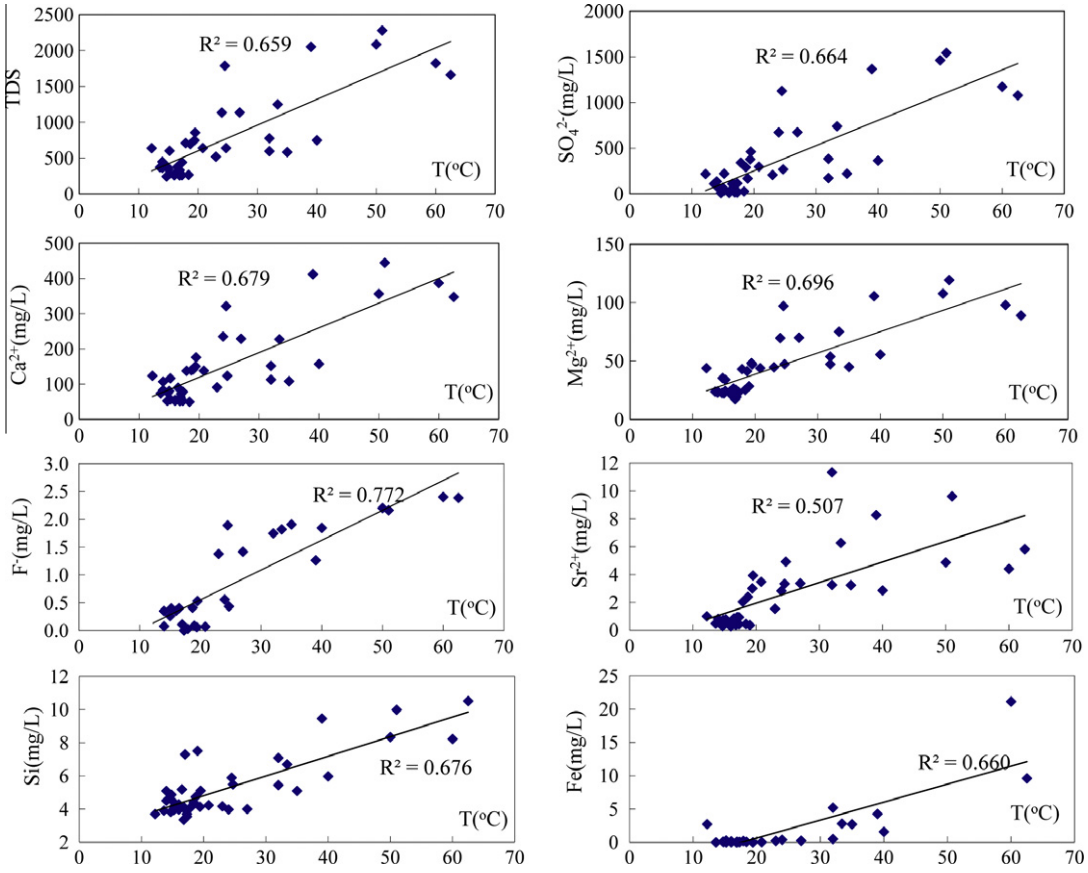

Fig. 4. Correlation between temperature and TDS, concentration of SO_4^{2-}, Ca^{2+}, Mg^{2+}, F^-, Si, Sr^{2+} and Fe in karst groundwater samples from Taiyuan.

respect to carbonate minerals while all the waters were found to be undersaturated with respect to gypsum, anhydrite, fluorite, celestite and strontianite, indicating a prevailing trend of dissolution of these sulfate and fluoride minerals in the aquifer systems. A common feature of the SI values with respect to different minerals is their general tendency to increase from the recharge towards the discharge zone and even further for the thermal karst groundwater discharge zone, whereby the latter increase reflects the more extensive dissolution of minerals within the discharge zones.

5. Discussion

5.1. Hydrogeochemical processes

Fig. 4 shows that the concentrations of TDS, SO_4^{2-}, Ca^{2+}, Mg^{2+}, F^-, Sr^{2+}, Si and Fe in groundwaters are positively correlated with temperature, indicating that the groundwater geochemistry of the carbonate aquifer is affected by temperature-related water–rock interaction.

5.1.1. Hydrogeochemical processes controlling Ca^{2+}, Mg^{2+}, HCO_3^- and SO_4^{2-} concentrations

Following rainwater recharge, the infiltrating water reacts with the major mineral phases in the aquifer, namely calcite, dolomite and gypsum. Dissolved Ca^{2+} concentrations may increase through the dissolution of carbonate minerals and/or gypsum. To distinguish the effect of carbonate and gypsum dissolution on karst groundwater hydrochemistry the following are considered: First, the dissolution reaction of gypsum is

$$CaSO_4 \rightarrow Ca^{2+} + SO_4^{2-} \quad (1)$$

By assuming that all the SO_4^{2-} in the groundwater of the study area is derived from gypsum dissolution the non-gypsum Ca^{2+} source can be determined by subtracting the amount of Ca^{2+} equivalent to the amount of SO_4^{2-} from the total Ca^{2+} concentration and expressed as $\{Ca^{2+}\}$–$\{SO_4^{2-}\}$ (in mmol/L) (Wang et al., 2006). The non-gypsum source Ca^{2+} is mainly from carbonate mineral dissolution.

5.1.1.1. Carbonate mineral dissolution. The congruent dissolution of calcite is

$$CaCO_3 + CO_{2(g)} + H_2O \leftrightarrow Ca^{2+} + 2HCO_3^- \quad (2)$$

while the stoichiometry of dolomite dissolution is:

$$CaMg(CO_3)_2 + 2CO_{2(g)} + 2H_2O \leftrightarrow Ca^{2+} + Mg^{2+} + 4HCO_3^- \quad (3)$$

and the simultaneous dissolution of calcite and dolomite is:

$$CaCO_3 + CaMg(CO_3)_2 + 3CO_{2(g)} + 3H_2O \leftrightarrow 2Ca^{2+} + Mg^{2+} + 6HCO_3^- \quad (4)$$

Accordingly the molar ratios for Ca^{2+}/HCO_3^- production in Eqs. (2)-(4) are 1/2, 1/4 and 1/3, respectively, while the molar ratios for Mg^{2+}/HCO_3^- for congruent dolomite dissolution and the combined dissolution of calcite and dolomite are 1/4 and 1/6, respectively.

The ratios of the non-gypsum sourced Ca^{2+} (Ca^{2+}–SO_4^{2-}) vs. HCO_3^- for the water samples from the BMK are plotted and they fall consistently between the 1:3 and the 1:4 lines (Fig. 5), while the ratios of Mg^{2+} vs. HCO_3^- all plot between the 1:4 and the 1:6 line

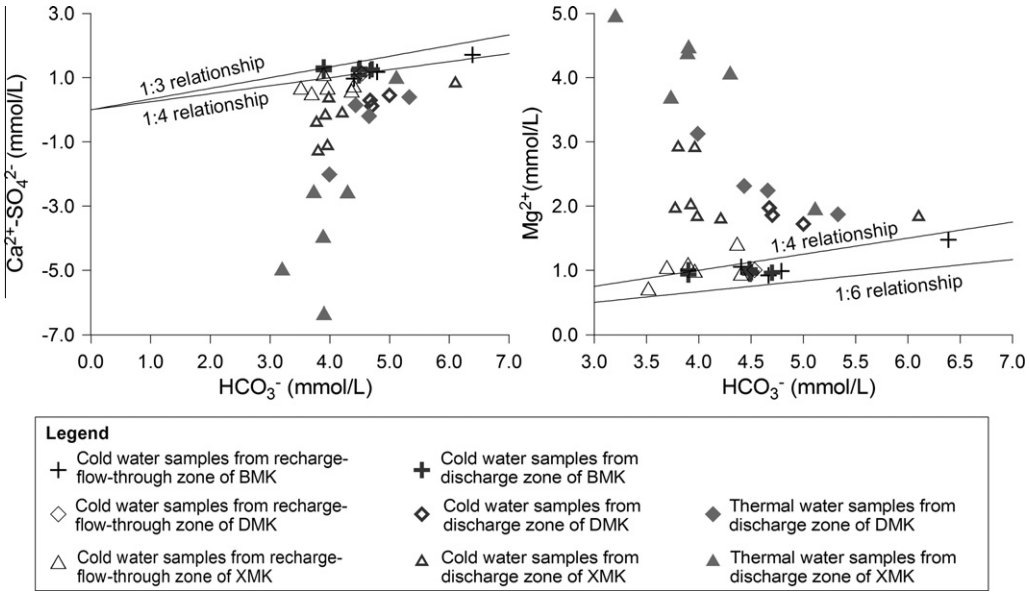

Fig. 5. Non-gypsum source Ca^{2+} vs. HCO_3^- concentrations (a) and Mg^{2+} vs. HCO_3^- concentrations (b) for karst groundwater samples in Taiyuan.

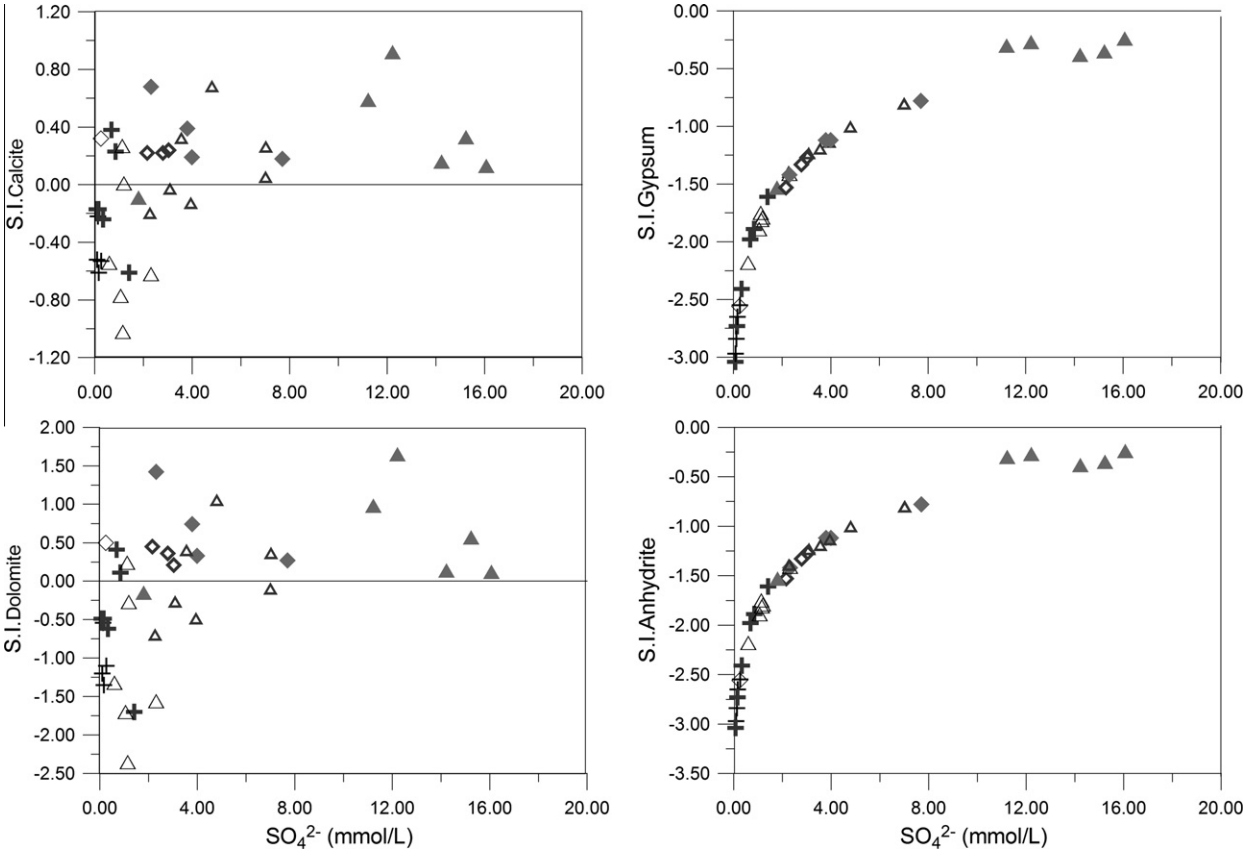

Fig. 6. Comparison of saturation indices (S.I.) with respect to calcite, dolomite, and gypsum as a function of SO_4^{2-} content. Symbols as in Fig. 5.

(Fig. 5). This provides strong evidence that the waters evolved from a net dissolution of calcite and dolomite in the BMK. The groundwater samples from the recharge and the flow-through zone of the DMK and the XMK also plot between the 1:3 and the 1:4 lines for non-gypsum sourced Ca^{2+} vs. HCO_3^- (Fig. 5). They plot especially close to the 1:4 line for non-gypsum Ca^{2+} vs. HCO_3^- while also plotting between the 1:4 and the 1:6 lines for Mg^{2+} vs. HCO_3^- (Fig. 5). This suggests that these water chemistries also originate from calcite and dolomite net dissolution with dolomite dissolution being the dominant process for the control of Ca^{2+} and HCO_3^- concentrations.

5.1.1.2. Dedolomitization. As the Ca^{2+} concentration increases in the water due to gypsum dissolution, the common ion effect may trig-

ger calcite over-saturation and precipitation, causing a decrease in Ca^{2+} and HCO_3^- concentrations. This leads in turn to an undersaturation (and dissolution) of dolomite, which then increases Mg^{2+} concentrations in the waters. Therefore, the "common ion effect" for Ca^{2+} from concurrent dissolution of gypsum may lead to the precipitation of calcite and the dissolution of dolomite. This process is known as dedolomitization.

Fig. 6 shows a comparison of calcite, dolomite, gypsum and anhydrite saturation indices of all water samples as a function of SO_4^{2-} concentration. It can be seen that along the flow path from the recharge zone towards the cold karst groundwater discharge zone, and further to the thermal karst groundwater discharge zone, the waters approach gypsum and anhydrite saturation as SO_4^{2-} concentrations increase steadily. The calcite and dolomite saturation indices also increase successively as SO_4^{2-} concentrations increase. Most waters sampled from the discharge zone of the XMK and the DMK were slightly oversaturated with respect to calcite, which points to a dedolomitization of the Taiyuan carbonate aquifer.

Dedolomitization driven by gypsum dissolution is a well recognized process, especially in carbonate systems containing evaporate sulphates (gypsum, anhydrite) (e.g., Back et al., 1983; Hanshaw and Back, 1979). It has been documented at a regional scale for numerous aquifers, e.g. the Madison aquifer (Plummer et al., 1990), Floridan aquifers (Wicks and Herman, 1994, 1996), Beuda and Perafita Formations, Spain (Bischoff et al., 1994), carbonate aquifers in the Betic Cordillera, Spain (López-Chicano et al., 2001), carbonate aquifers from the Mt Catria-Mt Nerone ridge, Northern Appennines, Italy (Capaccioni et al., 2001), the Carboniferous–Permian aquifer in the Unisław Śląski–Sokołowsko area (the Sudetes, Poland) (Dobrzyński, 2007) and the Silurian–Devonian carbonate aquifers in the Great Lakes region (McIntosh and Walter, 2006).

The systematic increase between the recharge zone towards the discharge zone in both Ca^{2+} and Mg^{2+} in conjunction with a SO_4^{2-} and CO_2 partial pressure increase, and a decrease in pH are characteristic consequences of dedolomitization reactions (Back et al., 1983; Plummer et al., 1990). The decrease in HCO_3^- is also a result stemming from the evolutionary paths following the dedolomitization reaction.

5.1.2. Hydrogeochemical processes controlling Cl^-, Na^+ and NO_3^- concentrations

The average contents of Cl^-, Na^+ and K^+ in the groundwaters from the Taiyuan carbonate aquifer are 17.5 mg/L, 22.34 mg/L and 2.44 mg/L, respectively. In the recharge area, the concentration of Cl^- in some waters is slightly higher, presumably indicating contamination from industrial and agricultural activities in this area. The linear relationship of Cl^- vs. Na^+ (Fig. 7) indicates that some of the Na^+ is likely to originate from halite dissolution. Since the ratio Na^+/Cl^- is commonly greater than unity (Fig. 7), the excess of Na^+ over Cl^- suggests additional contributions of Na^+ from other sources. For example, mixing with groundwater infiltrating from the Permian, which mainly consists of silicate minerals may also contribute to an increase of Na^+ and K^+ and hydrolysis of other minerals such as feldspar and muscovite may also account for more excessive Na^+ concentrations in the karst groundwaters.

The measured NO_3^- concentration ranged between 1.71 mg/L and 34.24 mg/L and decreased along the flow path (Table 1). In the recharge zones of the karst water sub-systems, the groundwater is open to direct seepage of contaminants. Normally aerobic conditions prevail in this zone. The higher concentrations of NO_3^- in this area are presumably caused by xenobiotic pollution. In contrast, the thick caps above the discharge zone protect the karst groundwater from contamination (Fig 1b). This is considered the most likely explanation for the decreasing trend of NO_3^- concentrations along the flow path. The occurrence of denitrification under the anaerobic conditions in the thermal groundwater discharge zone (suggested by the strong H_2S odor of sampled thermal groundwaters) is in principle also a possible explanation, which could cause the same NO_3^- concentration patterns.

5.1.3. Hydrogeochemical processes controlling F^- and Sr^{2+} concentrations

The F^- concentration of thermal karst groundwaters at Taiyuan is generally greater than 1 mg/L, much higher than those of cold karst groundwaters (Table 1). Higher temperatures in the thermal waters may be partly responsible for the observed higher F^- concentrations than that in cold waters since the solubility of fluorite increases with rising temperatures (Langmuir, 1997). Carbonate precipitation is another important factor affecting F^- enrichment

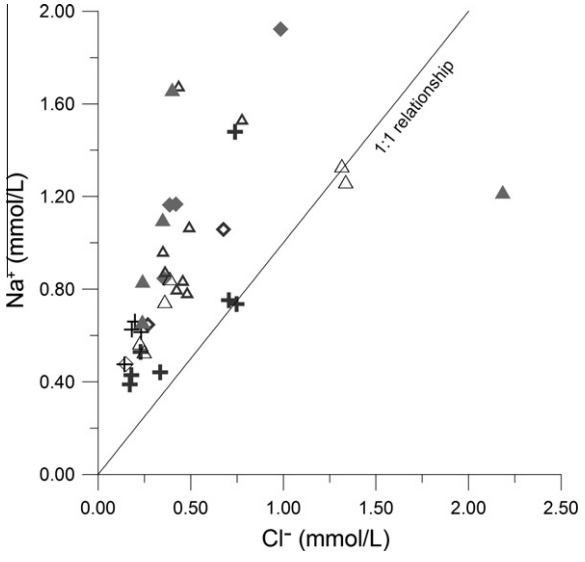

Fig. 7. Plot of Cl^- vs. Na^+ in karst groundwater samples. Symbols as in Fig. 5.

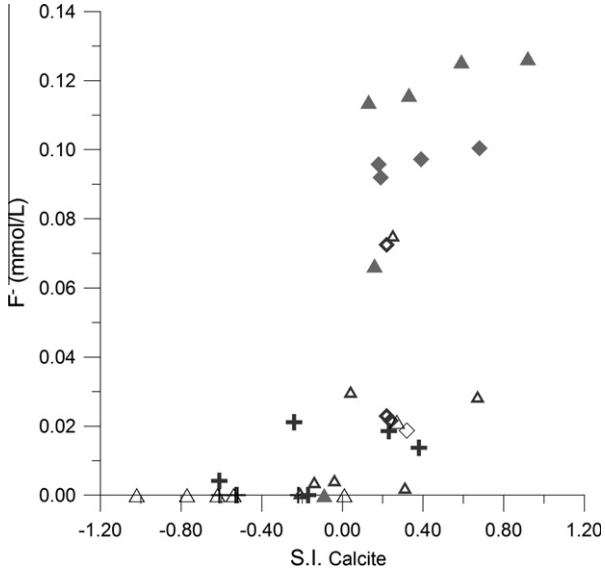

Fig. 8. Plot of F^- vs. S.I. with respect to calcite for karst groundwater samples. Symbols as in Fig. 5.

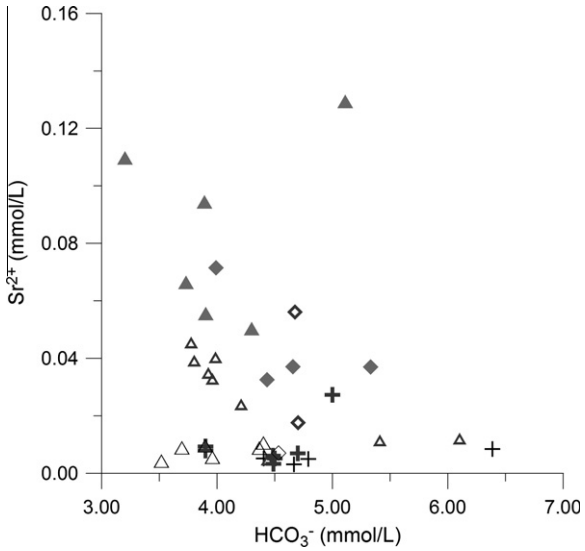

Fig. 9. Plot of Sr^{2+} vs. HCO_3^- in karst groundwater samples. Symbols as in Fig. 5.

in thermal karst groundwaters. Calcite precipitation in the discharge zone of the XMK and the DMK reduces Ca^{2+} concentrations, which then promotes the dissolution of fluorite. The negative relationship between calcite saturation index and F^- concentrations underpins the strong likelihood for the occurrence of this process (Fig. 8).

Sr^{2+} concentration increased greatly from the recharge zone towards the discharge zone and further to the thermal karst groundwater discharge zone (Table 1). Fig. 9 shows the strontianite solubility control on Sr enrichment in the karst groundwater. The dissolution of strontianite is, therefore, likely to be the major source of Sr in the karst groundwaters.

5.2. Mass balance reaction models

In order to further validate the conceptual hydrochemical model the above discussed reaction hypotheses were tested by constructing geochemical mass balance models for each subsystem (BMK, DMK and XMK) to quantitatively represent the changes in water composition between the recharge water and discharge water.

In the conceptual inverse mass balance model, waters from the recharge subgroups (in Table 1) form the "initial water" and waters from the discharge zone were defined as the "final" water. The waters in each zone, which were contaminated, or not located along the flow lines, or not measured for some minor elements, were eliminated (e.g., RN27, TY25, RN12, RN32, TY16 and TY17).

In the BMK, groundwater is assumed to flow from the recharge zone towards the flow-through zone to the margin of the mountain, and further to the buried carbonate aquifer in the basin. The corresponding simulated flow path was selected to be represented by the "initial water" (average of RN28, RN29, RN30 and RN31), the "intermediate water" (average of RN10, RN12 and RN13), and the "final water" (average of TY01, TY07 and TY08).

5.2.1. Plausible phases

The phases included in the mass balance modeling, were selected on the basis of the analysis of the chemical trends, calculated SI values, and the mineralogy. These are summarized in Table 3. Dolomite, calcite and gypsum were included to quantify the carbonate dissolution/precipitation, gypsum dissolution and dedolomitization reactions. Although the deep, confined groundwater system is expected to be closed with respect to CO_2 gas mass transfer, this does not preclude the possibility of reactions producing or consuming CO_2 within the aquifer (e.g. through carbonate mineral dissolution or precipitation), and entrance of CO_2 to the aquifer from an external source such as cross-formational leakage or release from the aquifer such as through outgassing. Thus, CO_2 was included among the plausible phases. Siderite occurs in the aquifer rocks and could be considered as the source phase of Fe. Strontianite and fluorite were included in the model as both are observed in the bedrock. Albite, K-feldspar and K-mica, respectively, were incorporated in the model as hypothetical sources to explain the increase in Na^+, K^+ and Al. Dissolution of halite was anticipated, as discussed earlier, and included in the simulation. Finally, quartz was considered in the model to explain variations of Si in the groundwater along the flow path.

Table 3
Selected phases for mass balance reaction modeling.

Phase	Composition
Calcite	$CaCO_3$
Dolomite	$CaMg(CO_3)_2$
Gypsum	$CaSO_4{\cdot}2H_2O$
Fluorite	CaF_2
CO_2 (g)	CO_2
Strontianite	$SrCO_3$
Siderite	$FeCO_3$
Quartz	SiO_2
Halite	NaCl
Albite	$NaAlSi_3O_8$
K-feldspar	$KAlSi_3O_8$
K-mica	$KAl_3Si_3O_{10}(OH)_2$

In all groundwaters from the BMK, the concentrations of Fe, F^- and Sr^{2+} is very small and the minerals containing these elements (Siderite, fluorite and strontianite), therefore, were not included in the inverse model for the BMK. As the changes in Na^+ and K^+ were very small, silicate minerals (Albite, K-feldspar and K-mica) were also excluded from the BMK model.

5.2.2. Criteria used in reaction modeling

As discussed earlier, the CO_2 gas mass transfer is expected to be near zero, and the magnitude of this term has been used as a criterion in refining the mass balance models. An uncertainty limit of 2.5% was assigned to all chemical data, except Cl^- for the initial water and final water in all karst groundwater systems. Chloride was assigned an uncertainty limit of 10% because of the contamination origin. An uncertainty limit of 50% and 100% was assigned to Na^+ and K^+ for inverse modeling of the BMK because the models did not include the phases containing these two elements.

5.2.3. Mass transfer results

The simulated mass transfer of calcite, dolomite, gypsum, CO_2 gas, halite, fluorite, quartz, strontianite, siderite, albite, K-feldspar and K-mica (in mmol/kg of water) are listed in Table 4. The data shown in Table 4 indicate that dedolomitization, that is, dissolution of gypsum and dolomite accompanied by precipitation of calcite, is the predominant process throughout the Ordovician aquifer controlling water quality evolution between the recharge and the discharge zone in the XMK as well as the DMK. The extent to which this process proceeds appears to be a function of both the travel distance and the availability of gypsum. Between the recharge and the shallow discharge zone, and further to the deep discharge zone of the XMK and also of the DMK, gypsum and dolomite are dissolved, while the quantity of precipitating calcite increases. The gypsum mass transfer via dissolution reaches 11.6 mmol/kg of water along the flow paths to the deep discharge zone in the XMK. In contrast, the waters from the BMK show little gypsum dissolution, indicating low abundance of the mineral there and/or

Table 4
Mole transfers in the geochemical models with minimum number of phases (mmol/kgw).

Karst water subsystem		Calcite	Dolomite	Gypsum	CO_2(g)	Halite	Fluorite	Quartz	Strotianite	Siderite	Albite	K-feldspar	K-mica
DMK	Cold water discharge zone	−1.98	0.798	1.96	0.645	0.155	0.0269	−0.0918	0.0106	0.00108	0.0	0.0464	−0.0164
	Thermal water discharge zone	−3.090	1.330	4.310	0.328	0.388	0.039	−1.370	0.038	0.031	0.412	0.2850	−0.2330
BMK	Cold water discharge zone at the margin of the mountain	0.0987	−0.102	0.0261	−0.696	0.0	–	−0.0051	–	–	–	–	–
	Cold water discharge zone in buried karst zone	0.0	−0.036	0.811	−0.178	0.404	–	0.0127	–	–	–	–	–
XMK	Cold water discharge zone	−2.48	1.35	4.11	0.0	0.0821	0.0087	−1.34	0.0273	0.00247	0.463	0.211	−0.225
	Thermal water discharge zone	−6.88	3.38	11.6	0.0	0.0	0.0528	−1.390	0.0692	0.2090	0.263	0.4770	−0.2460

Negative value for precipitation and positive for dissolution; – indicates that the minerals were not included in the inverse model.

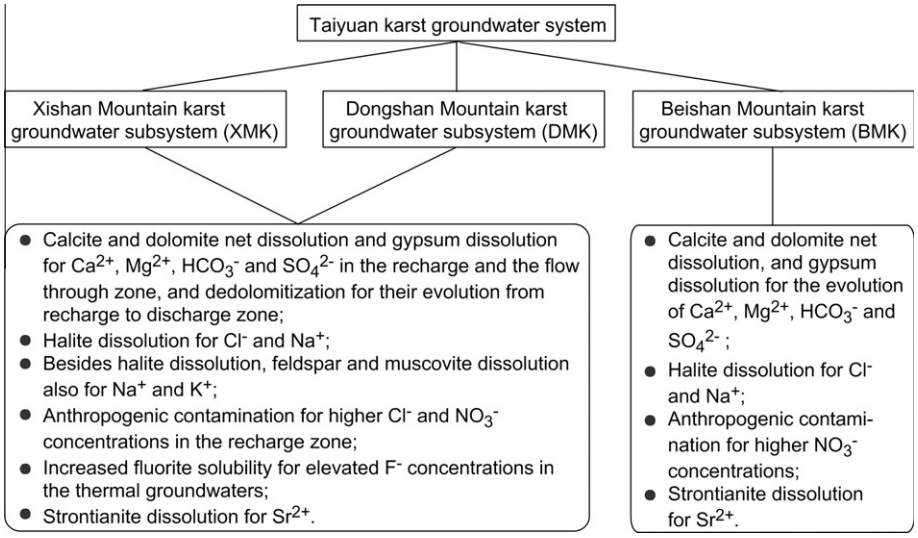

Fig. 10. Main geochemical processes controlling groundwater evolution in the Taiyuan karst groundwater system.

more rapid flow velocities. In the BMK mass transfer model only little dolomite precipitates and small amounts of calcite dissolve between the recharge zone and discharge zone at the margin of the mountains.

Near-zero values for the CO_2 gas mass transfer were expected for the deep, confined groundwater system. Indeed, the modeled CO_2 gas mass transfer for the XMK is 0.0 mmol/kg of water, which supports the assumption of the thermal karst groundwater system being a closed system. Calculated nonzero values for CO_2 gas mass transfer for the DMK and BMK may imply that CO_2 was produced or consumed through carbonate mineral dissolution/precipitation or that an external source such as cross-formational leakage was affecting concentrations. The deviations of CO_2 gas mass transfers from zero can be partly attributed to uncertainties in the composition of recharge waters or other errors in the modeling parameters used for the DMK and the BMK.

Halite dissolution and silicate mineral (albite, K-feldspar and K-mica) dissolution/precipitation are shown to be insignificant within the karst groundwater system, resulting from the presumed absence of halite and silicate minerals in the carbonate aquifer. The addition of albite and K-feldspar phases always accompanies quartz precipitation. The amount of fluorite, siderite and strontianite dissolution in the deep karst groundwater system exceeds that found for the shallow karst groundwater system and presumably reflects the longer travel distances of the groundwater from the deep karst groundwater system and the occurrence of higher temperatures which promoted dissolution rates.

The geochemical processes controlling groundwater evolution, obtained from the above data analysis and geochemical modeling results, are summarized in Fig. 10.

6. Summary and conclusions

In this study the hydrogeochemistry of the Xishan Mountain, Dongshan Mountain and Beishan Mountain karst groundwater sub-systems was systematically evaluated. Water samples were classified according to major ion contents and temperatures. From the recharge - flow-through zone, to the cold groundwater discharge zone, and further to the thermal groundwater discharge zone in the DMK and the XMK, the water type changes from HCO_3 to $HCO_3{\cdot}SO_4/SO_4{\cdot}HCO_3$, and to SO_4, temperature from 13–18 °C to 18–25 °C, and up to 62.5 °C, and TDS from less than 500 mg/L to about 1000 mg/L, and up to 2000 mg/L. The concentrations of SO_4^{2-}, Ca^{2+} and Mg^{2+} also increase along the groundwater flow path, while that of HCO_3^- decreases slightly. The concentrations of Sr^{2+}, Si, Fe, F^- and some trace elements increase with temperature. Flow system analysis of

the spatial distribution of the hydrogeochemical data show that the thermal water discharges from the regional groundwater flow system.

Based on the analysis of geochemical data conceptual hydrochemical models were constructed. The developed hypotheses on which geochemical processes control groundwater composition were subsequently validated by mass balance reaction models. These mass balance models provided consistent results.

The work shows that the hydrogeochemistry of the groundwaters in Taiyuan's carbonate aquifers is mainly controlled by water rock interaction. In the whole area of the BMK the major chemical composition (Ca^{2+}, Mg^{2+}, HCO_3^- and SO_4^{2-}) of the groundwaters was found to evolve from calcite and dolomite net dissolution in conjunction with gypsum dissolution. In the recharge area of the XMK and DMK, the water chemistries originate from both calcite and dolomite net dissolution and gypsum dissolution whereby dolomite dissolution is the dominant process for Ca^{2+} and HCO_3^- concentrations. The evolution of the groundwater hydrogeochemistry along the flow path in the XMK and the DMK is affected by both carbonate dissolution/precipitation and gypsum dissolution. From the recharge to the discharge zone of the XMK and the DMK, the Ca^{2+} common ion effect due to gypsum dissolution drives calcite to precipitate and dolomite to dissolve. Thus, dedolomitization is shown to be an important process for controlling the hydrogeochemical evolution of the groundwater in the XMK and the DMK. Na^+ and K^+ may be derived from feldspar and muscovite dissolution in addition to halite dissolution. Higher Cl^- and NO_3^- concentrations in the recharge zone indicate that some level of contamination has occurred. Higher temperatures and increased fluorite solubility due to carbonate precipitation are thought to be responsible for elevated F^- concentrations in the thermal groundwaters. Dissolution of strontianite appears to be the major source of Sr^{2+} in the waters.

Acknowledgements

This research was financially supported by National Natural Science Foundations of China (NSFC-41002081, NSFC-40702042 and NSFC-40830748). The work was also supported by MOE Key Laboratory of Biogeology and Environmental Geology, China University of Geosciences, Wuhan, China. We are grateful to two anonymous reviewers whose constructive comments have significantly improved the presentation of this work.

References

Back, W., Hanshaw, B.B., Plummer, L.N., Rahn, P.H., Rightmire, C.T., Rubin, M., 1983. Process and rate of dedolomitization: mass transfer and ^{14}C dating in a regional carbonate aquifer. Geol. Soc. Am. Bull. 94, 1414–1429.

Bischoff, J.L., Julia, R., Shanks III, W.C., Rosenbauer, R.J., 1994. Karstification without carbonic acid: bedrock dissolution by gypsum-driven dedolomitization. Geology 22, 995–998.

Capaccioni, B., Didero, M., Paletta, C., Salvadori, P., 2001. Hydrogeochemistry of groundwaters from carbonate formations with basal gypsiferous layers: an example from the Mt Catria-Mt Nerone ridge (Northern Appennines, Italy). J. Hydrol. 253, 14–26.

Dobrzyński, D., 2007. Chemical diversity of groundwater in the Carboniferous–Permian aquifer in the Unisław Śląski–Sokołowsko area (the Sudetes, Poland): a geochemical modeling approach. Acta Geol. Polonica 57, 97–112.

Grasby, S.E., Betcher, R.N., 2002. Regional hydrogeochemistry of the carbonate rock aquifer, southern Manitoba. Can. J. Earth Sci. 39, 1053–1063.

Ha, C., Tang, B., Lu, R., 1989. Characteristics of fissure karst in the middle Ordovician limestone and groundwater natural resources in the west mountain of Taiyuan, Shanxi Province. Carsologica Sinica 8, 41–46 (in Chinese).

Han, X., Lu, R., Li, Q., 1993. Karst Water System—Case Study of Big Karst Spring in Shanxi Prov. Geology Press, Beijing, China.

Hanshaw, B.B., Back, W., 1979. Major geochemical processes in the evolution of carbonate-aquifer systems. J. Hydrol. 43, 287–312.

He, Y., Xu, C., 1993. Study on block-type hydrogeological structure of interstratified limestone in Taiyuan Region. Carsologica Sinica 12, 55–66 (in Chinese).

He, Y., Wu, Q., Xu, C., 1997. Study of the Karstic Water-resources in Taiyuan Area. Tongji University Press, Shanghai, China (in Chinese with English abstract).

Hess, J.W., White, W.B., 1993. Groundwater geochemistry of the carbonate karst aquifer, southcentral Kentucky, USA. Appl. Geochem. 8, 189–204.

Jacobson, A.D., Wasserburg, G.J., 2005. Anhydrite and the Sr isotope evolution of groundwater in a carbonate aquifer. Chem. Geol. 214, 331–350.

Kohfahl, C., Sprenger, C., Herrera, J.B., Meyer, H., Chacón, F.F., Pekdeger, A., 2008. Recharge sources and hydrogeochemical evolution of groundwater in semiarid and karstic environments: a field study in the Granada Basin (Southern Spain). Appl. Geochem. 23, 846–862.

Langmuir, D., 1997. Aqueous Environmental Geochemistry. Prentice-Hall Inc., Upper Saddle River, New Jersey.

López-Chicano, M., Bouamama, M., Vallejos, A., Pulido-Bosch, A., 2001. Factors which determine the hydrogeochemical behaviour of karstic springs. A case study from the Betic Cordilleras, Spain. Appl. Geochem. 16, 1179–1192.

Ma, R., Wang, Y., Sun, Z., Ma, T., Zheng, C., submitted for publication. Identification of groundwater flow paths in a carbonate aquifer system based on hydrogeological, isotopic and temperature data. In: Zheng, C., Liu, J., Siegel, D. (Eds.), Hydrogeology and Water Resources of China. Geological Society of America Special Papers.

McIntosh, J.C., Walter, L.M., 2006. Paleowaters in Silurian–Devonian carbonate aquifers: geochemical evolution of groundwater in the Great Lakes region since the Late Pleistocene. Geochim. Cosmochim. Acta 70, 2454–2479.

Moral, F., Cruz-Sanjulián, J.J., Olías, M., 2008. Geochemical evolution of groundwater in the carbonate aquifers of Sierra de Segura (Betic Cordillera, southern Spain). J. Hydrol. 360, 281–296.

Parkhurst, D., Appelo, C., 1999. User's Guide to PHREEQC (Version 2) – A Computer Program for Speciation, Batch-reaction, One-Dimensional Transport, and Inverse Geochemical Calculations. US Geol. Surv. Water Resour. Invest. Rep. No. 99-4259.

Plummer, L.N., Busby, J.F., Lee, R.W., Hanshaw, B.B., 1990. Geochemical modeling of the madison aquifer in parts of Montana, Wyoming, and South Dakota. Water Resour. Res. 26, 1981–2014.

Stetzenbach, K.J., Farnham, I.M., Hodge, V.F., Johannesson, K.H., 1999. Using multivariate statistical analysis of groundwater major cation and trace element concentrations to evaluate groundwater flow in a regional aquifer. Hydrol. Process. 13, 2655–2673.

Wang, Y., Shpeyzer, G.M., 1997. Genesis of thermal groundwaters from Siping'an district, China. Appl. Geochem. 12, 437–445.

Wang, R., Wang, H., 1990. Recharge of karst groundwater in east mountain, Taiyuan. Carsologica Sinica 9, 1–6 (in Chinese).

Wang, Y., Guo, Q., Su, C., Ma, T., 2006. Strontium isotope characterization and major ion geochemistry of karst water flow, Shentou, northern China. J. Hydrol. 328, 592–603.

Wicks, C.M., Herman, J.S., 1994. The effect of a confining unit on the geochemical evolution of ground water in the Upper Floridian aquifer system. J. Hydrol. 153, 139–155.

Wicks, C.M., Herman, J.S., 1996. Regional hydrogeochemistry of a modern coastal mixing zone. Water Resour. Res. 32, 401–407.

Wu, T., 1997. Stratigraphy (Lithostratic) of Shanxi Province. China University of Geoscience Press, Wuhan, China (in Chinese with English abstract).

Xu, G., Ha, C., Wang, H., Wang, R., 1987. Karst fissure groundwater system in the western mountain, Taiyuan, Shanxi. J. Geomech. 2, 85–125 (in Chinese).

Zhang, S., 1990. The study on karst hydrogeological structure system in Taiyuan area, Shanxi Province. Chin. J. Geol. 25, 173–182 (in Chinese).

Zhang, D., 1993. Bedding karst and multilayered groundwater flows in karstic block mountains in the northeast of Mount Xishan, Taiyuan, China. Quart. J. Eng. Geol. 26, 205–216.

Zhao, Y., Cai, Z., 1990. Research on the Karst-water System: Case Study of Taiyuan Area. Science Press, Beijing, China (in Chinese with English abstract).